polymers

MDPI

Article

Heteronuclear Dirhodium-Gold Anionic Complexes: Polymeric Chains and Discrete Units

Estefania Fernandez-Bartolome [1], Paula Cruz [1], Laura Abad Galán [1], Miguel Cortijo [1], Patricia Delgado-Martínez [2], Rodrigo González-Prieto [1,*], José L. Priego [1] and Reyes Jiménez-Aparicio [1,*]

[1] Departamento de Química Inorgánica, Facultad de Ciencias Químicas, Universidad Complutense de Madrid, Ciudad Universitaria, E-28040 Madrid, Spain; estefania.fernandez@imdea.org (E.F.-B.); paula.cruz@urjc.es (P.C.); laura.abad-galan@ens-lyon.fr (L.A.G.); miguelcortijomontes@ucm.es (M.C.); bermejo@ucm.es (J.L.P.)

[2] Unidad de Difracción de Rayos X. Centro de Asistencia a la Investigación de Técnicas Físicas y Químicas. Universidad Complutense de Madrid. Ciudad Universitaria. E-28040 Madrid, Spain; patriciadelgado@ucm.es

* Correspondence: rodgonza@ucm.es (R.G.-P.); reyesja@quim.ucm.es (R.J.-A.)

Received: 31 July 2020; Accepted: 17 August 2020; Published: 19 August 2020

Abstract: In this article, we report on the synthesis and characterization of the tetracarboxylatodirhodium(II) complexes $[Rh_2(\mu\text{–}O_2CCH_2OMe)_4(THF)_2]$ (**1**) and $[Rh_2(\mu\text{–}O_2CC_6H_4\text{–}p\text{–}CMe_3)_4(OH_2)_2]$ (**2**) by metathesis reaction of $[Rh_2(\mu\text{–}O_2CMe)_4]$ with the corresponding ligand acting also as the reaction solvent. The reaction of the corresponding tetracarboxylato precursor, $[Rh_2(\mu\text{–}O_2CR)_4]$, with $PPh_4[Au(CN)_2]$ at room temperature, yielded the one-dimensional polymers $(PPh_4)_n[Rh_2(\mu\text{–}O_2CR)_4Au(CN)_2]_n$ (R = Me (**3**), CH_2OMe (**4**), CH_2OEt (**5**)) and the non-polymeric compounds $(PPh_4)_2\{Rh_2(\mu\text{–}O_2CR)_4[Au(CN)_2]_2\}$ (R = CMe_3 (**6**), $C_6H_4\text{–}p\text{–}CMe_3$ (**7**)). The structural characterization of **1**, **3·2CH$_2$Cl$_2$**, **4·3CH$_2$Cl$_2$**, **5**, **6**, and **7·2OCMe$_2$** is also provided with a detailed description of their crystal structures and intermolecular interactions. The polymeric compounds **3·2CH$_2$Cl$_2$**, **4·3CH$_2$Cl$_2$**, and **5** show wavy chains with Rh–Au–Rh and Rh–N–C angles in the ranges 177.18°–178.69° and 163.0°–170.4°, respectively. A comparative study with related rhodium-silver complexes previously reported indicates no significant influence of the gold or silver atoms in the solid-state arrangement of these kinds of complexes.

Keywords: dirhodium(II) compounds; dicyano-aurate complexes; heteronuclear; one-dimensional; rhodium-gold anionic chains; coordination polymers

1. Introduction

Dirhodium(II) tetracarboxylato complexes with formula $[Rh_2(\mu\text{–}O_2CR)_4]$ (R = alkyl or aryl) are an important part of the huge family of complexes with metal–metal bonds. They display a paddlewheel structure and a single metal–metal bond order due to their background electronic configuration is $\sigma^2\pi^4\delta^2\delta^{*2}\pi^{*4}$, which is responsible for their diamagnetic nature [1–3]. The properties and reactivity of these complexes and their derivatives make them very interesting compounds for the scientific community. Due to their potential applications, they have been studied in fields like catalysis [4–12], bioinorganic chemistry [13–17], metal organic frameworks (MOFs) [18,19], or gas absorption [20,21]. Metal-organic aerogels [22,23] and liquid crystals [24,25] can also be obtained using them as building blocks.

The structural diversity found in many of this kind of complexes must be also highlighted [12,20,21,26–33]. The axial sites of the paddlewheel structure are easily occupied by monodentate ligands, which has allowed the preparation of a large number of molecular compounds [1,2,34–37].

One-dimensional polymers [1,2,38–41] can be obtained by means of bridging ligands between the dirhodium(II) cores.

Several approaches can be found in the literature to obtain heterometallic one-dimensional polymers where different metal complexes connect the dirhodium units [42–50]. The valuable physicochemical properties of some of them, like paramagnetism [42,47], modulation of their electronic structures [43], or luminescence [49], turn this kind of polymers into very promising materials. However, the number of heterometallic coordination polymers based on rhodium(II) carboxylates is still scarce.

Moreover, there is also an extensive bibliography about the use of cyanidometallate complexes to construct heteronuclear coordination polymers. This interest is explained due to their structural variety and interesting properties such as magnetism or luminescence [51–58]. Following this strategy, our research group has reported the synthesis and characterization of several heterometallic complexes based on cyanidometallate ligands coordinated to the axial positions of the Rh_2^{4+} paddlewheel unit [59–61].

The reaction of the corresponding paddlewheel tetracarboxylatodirhodium with cyanidometallate complexes in solution at room temperature allowed the synthesis of polymeric chains with formula $K_n\{Rh_2(\mu\text{–}O_2CR)_4[Au(CN)_2]\}_n$ (R = Me, Et) [59], and, very recently, $(PPh_4)_n[Rh_2(\mu\text{–}O_2CR)_4Ag(CN)_2]_n$ (R = Me, Ph, CH_2OEt) [60] and $(PPh_4)_{2n}[\{Rh_2(\mu\text{–}O_2CMe)_4\}\{M(CN)_4\}]_n$ (M = Ni, Pd, Pt) [61]. A similar reaction led also to the formation of the non-polymeric complex $(PPh_4)_2\{Rh_2(\mu\text{–}O_2CCMe_3)_4[Ag(CN)_2]_2\}$ [60]. The presence of $[Au(CN)_2]^-$ in these kind of complexes opens the possibility of aurophilic interactions [62] as it is found in compound $K_n\{Rh_2(\mu\text{–}O_2CEt)_4[Au(CN)_2]\}_n$ which displays luminescence with a broad intense emission at 475 nm upon excitation at 360 nm [59]. However, in spite of their easy synthesis and their potential luminescent properties, the complexes $K_n\{Rh_2(\mu\text{–}O_2CR)_4[Au(CN)_2]\}_n$ (R = Me, Et) [59] are, to our knowledge, the only two examples of polymers based on dirhodium tetracarboxylates with dicyanidoaurate(I) as axial bridge. Moreover, differences in the supramolecular structures of these complexes cause also differences in the luminescent properties, as the methyl derivative do not show this feature due to its long Au···Au distances. This fact highlights the importance of increasing the number of this type of polymers that allow the study of the influence of the solid state arrangement in their properties. Additionally, the counterion plays also an important role on the crystal structure and possible supramolecular interactions. For example, the bulky tetraphenylphosphonium cation can form supramolecular architectures by means of phenyl–phenyl embraces [63,64].

Taking into account the antecedents mentioned above, in this article we report the synthesis, characterization, and structural description of three heterometallic dirhodium-gold polymeric complexes with the formula $(PPh_4)_n[Rh_2(\mu\text{–}O_2CR)_4Au(CN)_2]_n$ (R = Me (**3**), CH_2OMe (**4**), CH_2OEt (**5**)). The structure of the starting complex $[Rh_2(\mu\text{–}O_2CCH_2OMe)_4(THF)_2]$ (**1**) is also described. The same reactions conditions starting from $[Rh_2(\mu\text{–}O_2CCMe_3)_4(HO_2CCMe_3)_2]$ and $[Rh_2(\mu\text{–}O_2CC_6H_4\text{–}p\text{–}CMe_3)_4(OH_2)_2]$ (**2**) led to the non-polymeric complexes $(PPh_4)_2\{Rh_2(\mu\text{–}O_2CR)_4[Au(CN)_2]_2\}$ (R = CMe_3 (**6**), $C_6H_4\text{–}p\text{–}CMe_3$ (**7**)), respectively. The structural characterization of compounds **6** and **7** is also provided in this work. The comparison of complexes **3**, **5**, and **6** with their silver derivatives [60] allows the study of the influence of gold or silver atoms in the crystal structures. Intermolecular interactions have been carefully surveyed in order to find possible phenyl embraces between the phenyl rings or short Au···Au distances.

2. Materials and Methods

2.1. Materials

$[Rh_2(\mu\text{–}O_2CCH_2OEt)_4(HO_2CCH_2OEt)_2]$ [60] and $[Rh_2(\mu\text{–}O_2CCMe_3)_4(HO_2CCMe_3)_2]$ [65,66] were prepared following published procedures. $PPh_4[Au(CN)_2]$ was synthesized following the published method to obtain $PPh_4[Ag(CN)_2]$ [60]. A solution of 0.2 mmol (0.06 g) of $K[Au(CN)_2]$ in 4 mL of water was mixed with a solution of 0.2 mmol (0.08 g) of PPh_4Br in 8 mL of water and stirred for 5 min at room temperature. The white precipitate obtained was collected by filtration and washed with 15 mL

of water and 10 mL of diethyl ether (10 mL). Yield: 0.082 g (70%). The rest of the reagents and solvents were acquired from commercial sources and used as received without further purification.

2.2. Physical Measurements

The elemental analysis measurements were carried out at the Microanalytical Services of the Complutense University of Madrid. FTIR measurements were carried out in the 4000 to 650 cm^{-1} spectral range with a Perkin–Elmer Spectrum 100 equipped with an universal ATR accessory (PerkinElmer, Inc., Shelton, CT, USA).

2.3. Crystallography

Single-crystal X-ray diffraction measurements were carried out at room temperature using a Bruker Smart-CCD diffractometer (Bruker Corporation, Billerica, MA, USA) with a Mo Kα (λ = 0.71073 Å) radiation and a graphite monochromator. CCDC 2015497–2015501 and 2015886 contain the crystallographic data for the compounds described in this article. These data can be obtained free of charge from the Cambridge Crystallographic Data Centre via *www.ccdc.cam.ac.uk/data_request/cif*.

2.4. Synthesis

2.4.1. Synthesis of $[Rh_2(\mu–O_2CCH_2OMe)_4(THF)_2]$ (**1**)

A mixture of 0.68 mmol (0.30 g) of $[Rh_2(\mu–O_2CMe)_4]$ and 29.85 mmol (2.69 g, 2.29 mL) of methoxyacetic acid was stirred and heated at 120 °C for 30 min under nitrogen atmosphere. The mixture was allowed to cool and the sticky product obtained was triturated and washed with 2 × 25 mL of a 3:2 hexane/diethyl ether mixture to obtain a green solid. Single crystals of **1** were obtained after 3 days by slow diffusion of hexane into a solution of the solid in THF. Yield: 0.25 g (52%). Anal. Calcd. (%) for $[Rh_2(\mu–O_2CCH_2OMe)_4]$: C, 25.64; H, 3.59. Found (%): C, 25.88; H, 3.53. FT-IR (cm^{-1}): 2935w, 2829w, 1600vs, 1431m, 1407s, 1330s, 1278w, 1197m, 1158w, 1130m, 1093s, 1016w, 939m, 898m, 731s.

2.4.2. Synthesis of $[Rh_2(\mu–O_2CC_6H_4–p–CMe_3)_4(OH_2)_2]$ (**2**)

$[Rh_2(\mu–O_2CMe)_4]$ (0.09 mmol (0.04 g)) and 40.00 mmol (7.13 g) of 4–*tert*–butylbenzoic acid were mixed and heated under nitrogen atmosphere until the latter melted (~165 °C). The reaction was kept for 30 min and then let to cool down to room temperature. The turquoise solid obtained was collected from the bottom of the flask and washed with several 60 mL fractions of a 1:5 diethyl ether/petroleum ether mixture. Yield: 0.02 g (23%). Anal. Calcd. (%) for **2**: C, 55.59; H, 5.94. Found (%): C, 55.52; H, 5.74. FT-IR (cm^{-1}): 3416w, 2963m, 2906w, 2869w, 1607m, 1589m, 1546m, 1466w, 1391s, 1268m, 1192m, 1148w, 1109w, 1016m, 856m, 781m, 731m, 712m.

2.4.3. Synthesis of $(PPh_4)_n[Rh_2(\mu–O_2CMe)_4Au(CN)_2]_n$ (**3**)

A 7 mL THF solution of 0.18 mmol (0.08 g) of $[Rh_2(\mu–O_2CMe)_4]$ was mixed with a 12 mL THF solution of 0.19 mmol (0.11 g) of $PPh_4[Au(CN)_2]$ and stirred for 1 day at room temperature obtaining a purple precipitate. The solid was filtered and washed with THF. Yield: 0.08 g (43%). Anal. Calcd. (%) for **3**: C, 39.63; H, 3.13; N, 2.72. Found (%): C, 39.78; H, 3.16; N, 2.79. FT-IR (cm^{-1}): 3083w, 2173w, 1598s, 1484w, 1409s, 1342m, 1163w, 1109s, 1042m, 997m, 753m, 721s, 688s.

The solid was dissolved in dichloromethane and THF was slowly added on top of the solution. Violet single crystals of **3·2CH$_2$Cl$_2$** were obtained after 2 days.

2.4.4. Synthesis of $(PPh_4)_n[Rh_2(\mu–O_2CCH_2OMe)_4Au(CN)_2]_n$ (**4**)

The synthesis was similar to the synthesis of **3** although in this case a solution of 0.11mmol (0.08 g) of $[Rh_2(\mu–O_2CCH_2OMe)_4(THF)_2]$ (**1**) in 5 mL of methanol and a solution of 0.12 mmol (0.07 g) of $PPh_4[Au(CN)_2]$ in 8 mL of THF were employed. The mixture was stirred for 30 min obtaining a purple solution. The solvent was evaporated and the solid obtained was washed with cold THF. Yield: 0.05

g (40%). Anal. Calcd. (%) for **4**: C, 39.67; H, 3.50; N, 2.43. Found (%): C, 40.03; H, 3.62; N, 2.31. FT-IR (cm^{-1}): 2822w, 2139w, 1608s, 1484w, 1435m, 1412m, 1330m, 1189w, 1162w, 1109vs, 1027w, 996w, 924w, 849w, 752w, 732vs, 687s.

Single crystals of **4·3CH$_2$Cl$_2$** suitable for X-ray diffraction were obtained after 4 days by slow diffusion of hexane into a solution of the compound in 4 mL of dichloromethane.

2.4.5. Synthesis of $(PPh_4)_n[Rh_2(\mu\text{–}O_2CCH_2OEt)_4Au(CN)_2]_n$ (**5**)

The synthesis was analogous to that of **3** using 8 mL of a THF solution of 0.07 mmol (0.06 g) of $[Rh_2(\mu\text{–}O_2CCH_2OEt)_4(HO_2CCH_2OEt)_2]$ and 0.10 mmol (0.06 g) of $PPh_4[Au(CN)_2]$ in 12 mL of THF. The purple solid obtained was washed with THF. Yield: 0.07 g (83%). Anal. Calcd. (%) for **5**: C, 41.81; H, 4.01; N, 2.32. Found (%): C, 41.58; H, 3.98; N, 2.39. FT-IR (cm^{-1}): 3074w, 2966m, 2925m, 2161m, 1612s, 1485m, 1433s, 1407s, 1363m, 1320s, 1260m, 1163m, 1135s, 1107s, 1032m, 1008m, 998m, 894w, 851m, 756m, 724s, 694s.

Purple single crystals of **5** were obtained after 2 days by slow diffusion of diethyl ether in a dichloromethane solution of the compound.

2.4.6. Synthesis of $(PPh_4)_2\{Rh_2(\mu\text{–}O_2CCMe_3)_4[Au(CN)_2]_2\}$ (**6**)

The synthesis was analogous to that of **3** using a solution of 0.10 mmol (0.08 g) of $[Rh_2(\mu\text{–}O_2CCMe_3)_4(HO_2CCMe_3)_2]$ in 10 mL of diethyl ether and a solution of 0.10 mmol (0.06 g) of $PPh_4[Au(CN)_2]$ in 8 mL of acetone. Yield: 0.034 g (38%). Anal. Calcd. (%) for **6**: C, 48.39; H, 4.29; N, 3.14. Found (%): C, 47.58; H, 4.20; N, 3.16. FT-IR (cm^{-1}): 3061w, 2968w, 2932w, 2866w, 2148w, 1576s, 1482s, 1458m, 1439s, 1412s, 1373m, 1361m, 1220s, 1107s, 997m, 935s, 894w, 802w, 781w, 763m, 723s, 690s.

Purple single crystals of **6** were obtained by slow evaporation of a solution of the solid in a 1:1 acetone/diethyl ether mixture.

2.4.7. Synthesis of $(PPh_4)_2\{Rh_2(\mu\text{–}O_2CC_6H_4\text{–}p\text{–}CMe_3)_4[Au(CN)_2]_2\}$ (**7**)

The synthesis was analogous to that of **3** but using dichloromethane solutions of the reactants 0.10 mmol (0.09 g) of $[Rh_2(\mu\text{–}O_2CC_6H_4\text{–}p\text{–}CMe_3)_4(OH_2)_2]$ (**2**) and 0.10 mmol (0.06 g) of $PPh_4[Au(CN)_2]$. A solution was obtained after the reaction, the solvent was evaporated, and a purple solid was obtained and washed with a dichloromethane/petroleum ether mixture. Yield: 0.07 g (67%). Anal. Calcd. (%) for **7**·2CH_2Cl_2: C, 52.05; H, 4.28; N, 2.25. Found (%): C, 52.58; H, 4.75; N, 2.48. FT-IR (cm^{-1}): 3058w, 2961m, 2906w, 2866w, 2161w, 1595s, 1556m, 1484w, 1474w, 1462w, 1437m, 1393s, 1268m, 1190m, 1149w, 1107s, 1017m, 997w, 855m, 780m, 755w, 722s, 712s, 689s.

Single crystals of $(PPh_4)_2\{Rh_2(\mu\text{–}O_2CC_6H_4\text{–}p\text{–}CMe_3)_4[Au(CN)_2]_2\}\cdot 2OCMe_2$ (**7·2OCMe$_2$**) were obtained after 7 days by slow diffusion of hexane into a solution of the compound in acetone in the fridge.

3. Results and Discussion

3.1. Synthesis of the Complexes

Complexes **1**–**7** have been obtained following the routes indicated in Scheme 1.

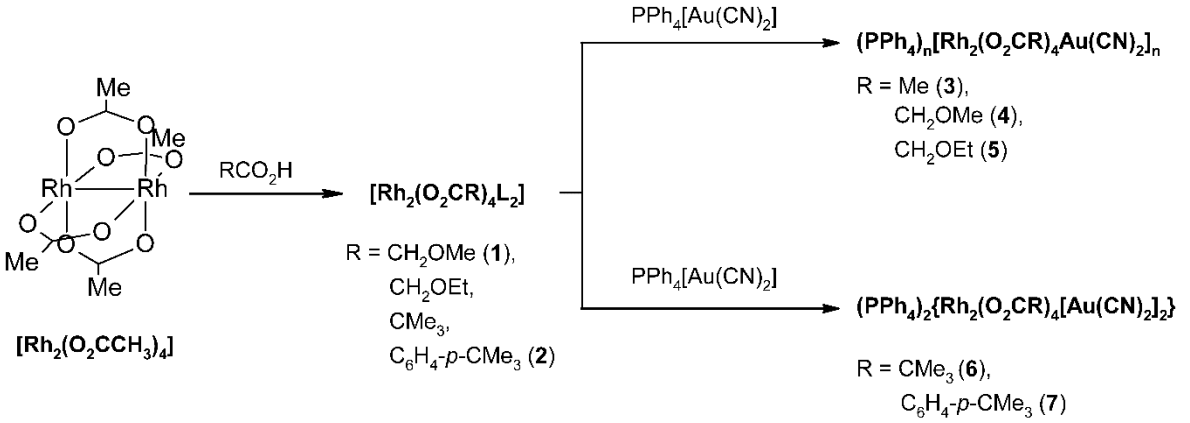

Scheme 1. Synthetic route for the synthesis of compounds **1**–**7**.

The metathesis reaction of $[Rh_2(\mu–O_2CMe)_4]$ in methoxyacetic acid led to the formation of $[Rh_2(\mu–O_2CCH_2OMe)_4(THF)_2]$ (**1**) after the removal of the excess ligand, washing with hexane and diethyl ether and crystallization process in THF. A similar reaction with melted 4–*tert*–butylbenzoic acid yielded complex $[Rh_2(\mu–O_2CC_6H_4–p–CMe_3)_4(OH_2)_2]$ (**2**) after washing with a mixture of diethyl ether and petroleum ether to eliminate the huge excess of solid ligand. The low solubility of the 4–*tert*–butylbenzoic acid in the washing mixture made necessary the use of a large volume of solvent. This synthetic method using the ligand as the reaction solvent is similar to the one used for the synthesis of $[Rh_2(\mu–O_2CCH_2OEt)_4(HO_2CCH_2OEt)_2]$ [60] and $[Rh_2(\mu–O_2CCMe_3)_4(HO_2CCMe_3)_2]$ [65,66]. Slow diffusion of different solvents into solutions of the complexes **1** and **2** was tested in order to get single crystals to allow the structural determination of these compounds. Single crystals of **1** were obtained using hexane and a solution of the solid obtained in THF. Unfortunately, all the attempts to obtain single crystals of **2** were unsuccessful. Nevertheless, the paddlewheel structure of complex **2** with four 4–*tert*–butylbenzoate bidentate ligands is proved in the crystal structure of complex **7** (see below).

One-dimensional polymeric complexes, $(PPh_4)_n[Rh_2(\mu–O_2CMe)_4Au(CN)_2]_n$ (**3**), $(PPh_4)_n[Rh_2(\mu–O_2CCH_2OMe)_4Au(CN)_2]_n$ (**4**), and $(PPh_4)_n[Rh_2(\mu–O_2CCH_2OEt)_4Au(CN)_2]_n$ (**5**), were obtained by stirring at room temperature solutions of the corresponding tetracarboxylato dirhodium complex with a solution of $PPh_4[Au(CN)_2]$ in THF. For compounds **3** and **5**, THF solutions were employed and these compounds were obtained as precipitates from the reaction mixture. For compound **4**, the chosen solvent was methanol and the solid was obtained after removal of the solvent mixture. Single crystals of the three complexes were obtained from slow diffusion of different solvents into dichloromethane solutions of the solids. In this way, THF was used to obtain single crystals of $\{(PPh_4)[Rh_2(\mu–O_2CMe)_4Au(CN)_2]\cdot 2CH_2Cl_2\}_n$ (**3·2CH$_2$Cl$_2$**), hexane for $\{(PPh_4)[Rh_2(\mu–O_2CCH_2OMe)_4Au(CN)_2]\cdot 3CH_2Cl_2]\}_n$ (**4·3CH$_2$Cl$_2$**), and diethyl ether for $(PPh_4)_n[Rh_2(\mu–O_2CCH_2OEt)_4Au(CN)_2]_n$ (**5**). Single crystals of compound **5**, with the same unit cell, were also obtained by slow diffusion of diethyl ether in an acetone solution of the compound.

Similar reactions at room temperature were employed to obtain the non-polymeric complexes $(PPh_4)_2\{Rh_2(\mu–O_2CCMe_3)_4[Au(CN)_2]_2\}$ (**6**) and $(PPh_4)_2\{Rh_2(\mu–O_2CC_6H_4–p–CMe_3)_4[Au(CN)_2]_2\}$ (**7**). An acetone solution of $PPh_4[Au(CN)_2]$ was stirred with a solution of $[Rh_2(\mu–O_2CCMe_3)_4(HO_2CCMe_3)_2]$ in diethyl ether to obtain compound **6**. Dichloromethane solutions of $PPh_4[Au(CN)_2]$ and **2** achieved compound **7** after evaporation of the solvent. Single crystals of **6** were formed after evaporation of a solution of the complex in acetone/diethyl ether, whereas layering hexane on top of an acetone solution of **7** and kept in the fridge (7 days) yielded single crystals of $(PPh_4)_2\{Rh_2(\mu–O_2CC_6H_4–p–CMe_3)_4[Au(CN)_2]_2\}\cdot 2OCMe_2$ (**7·2OCMe$_2$**).

The reaction conditions used for the synthesis of compounds **3**–**7** are analogous to those employed for the synthesis of the polymeric complexes $(PPh_4)_n[Rh_2(\mu–O_2CR)_4Ag(CN)_2]_n$ (R = Me, Ph, CH_2OEt) and the non-polymeric compound, $(PPh_4)_2\{Rh_2(\mu–O_2CCMe_3)_4[Ag(CN)_2]_2\}$ recently reported

by our research group [60]. This lead to crystals structures showing numerous structural similarities (see below).

3.2. IR Characterization

The IR spectrum of each compound shows the characteristic bands of the carboxylate ligands coordinated to the dimetallic unit. Thus, the infrared spectra of the seven compounds show the corresponding bands of the antisymmetric and symmetric stretching modes of the carboxylate groups: $\nu(COO)_a$ (1612–1576 cm^{-1}) and $\nu(COO)_s$ (1412–1391 cm^{-1}). The separation between the symmetric and antisymmetric bands indicates the symmetrical bridging coordination mode of the equatorial carboxylate ligands [67].

For complexes **3**–**7**, an additional band corresponding to the $\nu(C{\equiv}N)$ vibration is also visible in the 2173 to 2139 cm^{-1} range, indicating the presence of the $[Au(CN)_2]$ in the complexes.

3.3. Crystal Structures and Refinement Data

A summary of some crystal and refinement data obtained for complexes **1**, **3·2CH$_2$Cl$_2$**, **4·3CH$_2$Cl$_2$**, **5**, **6**, and **7·2OCMe$_2$** is shown in Table 1. More detailed information can be found in Tables S1–S6 and Figures S1–S6 in the Supporting Information.

Table 1. Crystal and refinement data for compounds **1**, **3·2CH$_2$Cl$_2$**, **4·3CH$_2$Cl$_2$**, **5**, **6**, and **7·2OCMe$_2$**.

	1	**3·2CH$_2$Cl$_2$**	**4·3CH$_2$Cl$_2$**	**5**	**6**	**7·2OCMe$_2$**
Formula	$C_{20}H_{36}O_{14}Rh_2$	$C_{36}H_{36}AuCl_4N_2O_8PRh_2$	$C_{41}H_{46}Cl_6AuN_2O_{12}PRh_2$	$C_{42}H_{48}AuN_2O_{12}PRh_2$	$C_{72}H_{76}Au_2N_4O_8P_2Rh_2$	$C_{102}H_{104}Au_2N_4O_{10}P_2Rh_2$
fw	706.31	1200.22	1405.25	1206.58	1787.06	2207.59
Space group	*P*-1	*P*-1	*P*-1	$P2_1/c$	*P*-1	*P*-1
a/ Å	8.0729(19)	13.0075(13)	12.9715(16)	13.180(2)	12.1505(10)	13.284(3)
b/ Å	12.380(3)	13.0075(13)	13.806(2)	22.270(4)	12.4592(10)	14.299(3)
c/ Å	14.900(4)	13.7398(15)	15.990(3)	16.901(3)	14.1408(12)	14.785(3)
α/ °	112.271(4)	87.339(2)	79.123(16)	90	70.0030(10)	99.189(4)
β/ °	90.008(4)	78.375(2)	86.132(15)	112.224(3)	69.4540(10)	110.244(3)
α/ °	92.332(4)	80.295(2)	71.808(18)	90	69.8730(10)	110.982(3)
V/ Å^3	1376.7(6)	2351.3(4)	2671.5(7)	4592.3(13)	1821.6(3)	2327.8(8)
Z	2	2	2	4	1	1
d calc/ *g*·cm^{-3}	1.704	1.695	1.747	1.748	1.629	1.575
μ /mm^{-1}	1.262	4.112	3.735	3.993	4.557	3.585
R indices	R_1 = 0.0351 wR_2 =0.0855	R_1 = 0.0459 wR_2 = 0.1559	R_1 = 0.0557 wR_2 = 0.1771	R_1 = 0.0433 wR_2 = 0.1171	R_1 = 0.0253 wR_2 = 0.0622	R_1 = 0.0659 wR_2 = 0.1334
GooF on F^2	0.918	0.993	0.992	0.989	1.045	0.997

$[Rh_2(\mu{-}O_2CCH_2OMe)_4(THF)_2]$ (**1**), $\{(PPh_4)[Rh_2(\mu{-}O_2CMe)_4Au(CN)_2]{\cdot}2CH_2Cl_2\}_n$ (**3·2CH$_2$Cl$_2$**), $\{(PPh_4)[Rh_2(\mu{-}O_2CCH_2OMe)_4Au(CN)_2]{\cdot}3CH_2Cl_2]\}_n$ (**4·3CH$_2$Cl$_2$**), $(PPh_4)_2\{Rh_2(\mu{-}O_2CCMe_3)_4[Au(CN)_2]_2\}$ (**6**), and $(PPh_4)_2\{Rh_2(\mu{-}O_2CC_6H_4{-}p{-}CMe_3)_4[Au(CN)_2]_2\}{\cdot}2OCMe_2$ (**7·2OCMe$_2$**) crystallize in the triclinic *P-1* space group, while $(PPh_4)_n[Rh_2(\mu{-}O_2CCH_2OEt)_4Au(CN)_2]_n$ (**5**) crystallizes in the monoclinic $P2_1/c$ space group. Compounds **3·2CH$_2$Cl$_2$** and **5** crystallize in the same space groups with similar cell parameters than the related dicyanidoargentate(I) complexes $\{(PPh_4)[Rh_2(\mu{-}O_2CMe)_4Ag(CN)_2]{\cdot}2CH_2Cl_2\}_n$ and $(PPh_4)_n[Rh_2(\mu{-}O_2CCH_2OEt)_4Ag(CN)_2]_n$ [60]. However, **6** crystallizes in a different space group than $(PPh_4)_2\{Rh_2(\mu{-}O_2CCMe_3)_4[Ag(CN)_2]_2\}$, which crystallizes in the orthorhombic *Pnma* space group [60].

The asymmetric unit of **1** contains two halves of two different paddlewheel units with inversion centers placed in between the M–M axis (Figure S1). Similarly, the asymmetric unit of both complexes **6** and **7·2OCMe$_2$** contains only one half of a paddlewheel unit and the other half is generated in the unit cell by an inversion center located in the center of the M–M axis. A tetraphenylphosphonium

cation in both structures and one acetone molecule in **7·2OCMe$_2$** complete the asymmetric unit of these compounds (Figures S5 and S6).

The asymmetric unit of **3·2CH$_2$Cl$_2$** and **4·3CH$_2$Cl$_2$** and **5** is formed by a tetraphenylphosphonium cation and a negatively charged tetracarboxylatodirhodium(II) unit with a dicyanidoaurate(I) ligand in one axial position. Additionally, dichloromethane molecules complete the asymmetric unit of **3·2CH$_2$Cl$_2$** and **4·3CH$_2$Cl$_2$** (see Figures S2–S4). The quality of the data allowed to model isotropically two and three dichloromethane molecules in **3·2CH$_2$Cl$_2$** and **4·3CH$_2$Cl$_2$**, respectively. The Platon Squeeze Routine [68] was used to remove additional disordered electron density in the structure of **3·2CH$_2$Cl$_2$**.

All the Rh(II) ions display a slightly distorted octahedral geometry, with the four equatorial positions occupied by oxygen atoms of the carboxylate ligands and the axial positions occupied by another Rh(II) ion, and the oxygen atom of a THF molecule in the case of **1**, and a nitrogen atom of a dicyanidoaurate(I) ligand in the case of **3·2CH$_2$Cl$_2$**, **4·3CH$_2$Cl$_2$**, **5**, **6**, and **7·2OCMe$_2$**. Rh-O$_{equatorial}$ distances are in the 1.989(1) to 2.063(5) Å range. Octahedra are axially elongated with Rh-O$_{axial}$ distances of 2.256(3) and 2.258(3) Å for **1**, Rh-N$_{axial}$ distances of 2.221(7) and 2.223(7) Å for **3·2CH$_2$Cl$_2$**, 2.209(8) and 2.187(9) Å for **4·3CH$_2$Cl$_2$**, 2.249(6) and 2.238(5) Å for **5**, 2.226(4) Å for **6** and 2.291(11) Å for **7·2OCMe$_2$**, and Rh-Rh distances of 2.3787(8) and 2.3810(8) Å for **1**, 2.3981(9) Å for **3·2CH$_2$Cl$_2$**, 2.4096(11) Å for **4·3CH$_2$Cl$_2$**, 2.4133(8) Å for **5**, 2.4002(6) Å for **6** and 2.3969(19) Å for **7·2OCMe$_2$**. All the Rh-Rh distances are indicative of a single bond between Rh(II) ions. Rh-Rh and Rh-N distances are similar to those found in other related compounds such as (PPh$_4$)$_{2n}$[{Rh$_2$(μ–O$_2$CCH$_3$)$_4$}{M(CN)$_4$}]$_n$ (M = Ni, Pd, Pt) [61], K$_n$[Rh$_2$(μ–O$_2$CR)$_4$Au(CN)$_2$]$_n$ (R = Me, Et) [59], (PPh$_4$)$_n$[Rh$_2$(μ–O$_2$CR)$_4$Ag(CN)$_2$]$_n$ (R = Me, Ph, CH$_2$OEt) [60], (PPh$_4$)$_2${Rh$_2$(μ–O$_2$CCMe$_3$)$_4$[Ag(CN)$_2$]$_2$} [60], [K(18–crown–6)(H$_2$O)]$_{2n}$[K(18–crown–6)(H$_2$O)$_2$]$_n$[Rh$_2$(μ–O$_2$CPh)$_4$Fe(CN)$_6$]$_n$·8nH$_2$O [69], and K$_{3n}${[Rh$_2$(μ–O$_2$CCH$_3$)$_4$]$_2$Co(CN)$_6$}$_n$ [70].

The structure of **3·2CH$_2$Cl$_2$, 4·3CH$_2$Cl$_2$**, and **5** is formed by chains constructed, respectively, by the following repetitive anionic units; [Rh$_2$(μ–O$_2$CMe)$_4$Au(CN)$_2$]$^-$, [Rh$_2$(μ–O$_2$CCH$_2$OMe)$_4$Au(CN)$_2$]$^-$, and [Rh$_2$(μ-O$_2$CCH$_2$OEt)$_4$Au(CN)$_2$]$^-$. A representation of the polymeric structure observed in **3·2CH$_2$Cl$_2$** is shown in Figure 1a as an example. On the other hand, the structure of **1**, **6**, and **7·2OCMe$_2$** is formed by discrete [Rh$_2$(μ–O$_2$CCH$_2$OMe)$_4$(THF)$_2$], {Rh$_2$(μ–O$_2$CCMe$_3$)$_4$[Au(CN)$_2$]$_2$}$^{2-}$, and {Rh$_2$(μ–O$_2$CC$_6$H$_4$–*p*–CMe$_3$)$_4$[Au(CN)$_2$]$_2$}$^{2-}$ units, respectively. The anionic paddlewheel unit of the structure of **6** is shown in Figure 1b. The crystal structure of complex **6** is similar to its analogous compound (PPh$_4$)$_2${Rh$_2$(μ–O$_2$CCMe$_3$)$_4$[Ag(CN)$_2$]$_2$}, whose molecular nature has been explained by a higher solubility of the branched trimethylacetate group in acetone, favoring the formation of a molecular complex due to a slower crystallization [60]. This fact is also corroborated by the obtaining of discrete anionic {Rh$_2$(μ–O$_2$CC$_6$H$_4$–*p*–CMe$_3$)$_4$[Au(CN)$_2$]$_2$}$^{2-}$ units in complex **7**, due to the also branched 4–*tert*–butylbenzoate ligand. A view of the packing of the discrete dirhodium units of **6** and **7·2OCMe$_2$** is shown in Figures S7 and S8 in the Supporting Information.

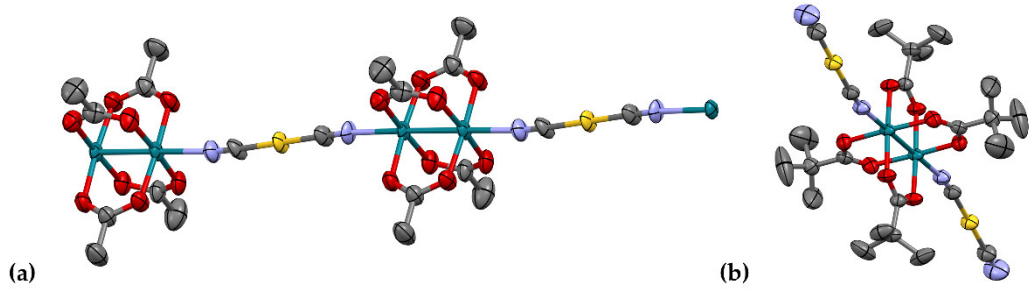

Figure 1. Representation (50% probability ellipsoids) of the chain formed by [Rh$_2$(μ-O$_2$CMe)$_4$Au(CN)$_2$]$^-$ repetitive units that is observed in the structure of **3·2CH$_2$Cl$_2$** (**a**) and the {Rh$_2$(μ-O$_2$CCMe$_3$)$_4$[Au(CN)$_2$]$_2$}$^{2-}$ units present in the structure of **6** (**b**). Rhodium: turquoise; oxygen: red; carbon: grey; nitrogen: purple; gold: yellow. Hydrogen atoms are omitted for clarity.

The anionic chains of **3·2CH$_2$Cl$_2$**, **4·3CH$_2$Cl$_2$**, and **5** have a wavy structure with Rh-Au-Rh angles of 178.69(1), 177.99(2), and 177.18(1), respectively, and Rh–N–C angles of 169.8(8) and 170.2(8) for **3·2CH$_2$Cl$_2$**, 170.4(10) and 167.7(10) for **4·3CH$_2$Cl$_2$** and 164.2(7) and 163.0(6) for **5**. This wavy structure

is analogous to those found in the related compounds $(PPh_4)_n[Rh_2(\mu\text{–}O_2CR)_4Ag(CN)_2]_n$ (R = Me, Ph, CH_2OEt) [60] with very similar values for the Rh-M-Rh (M = Ag, Au) and Rh–N–C angles when complexes with the same equatorial ligand are compared. These angles make that the wavy structures for compounds with R = CH_2OEt are more pronounced that for those with R = Me.

The anionic chains of **3·2CH_2Cl_2** and **4·3CH_2Cl_2** are packed parallel to each other along the *a* axis with the tetraphenylphosphonium cations and dichloromethane molecules between them. The chains of **3·2CH_2Cl_2** are arranged in pairs with each pair surrounded by other four pairs of chains (Figure 2a) in a similar way than the structure found for $\{(PPh_4)[Rh_2(\mu\text{–}O_2CMe)_4Ag(CN)_2]\cdot 2CH_2Cl_2\}_n$ [60], while the chains are arranged in rows in the structure of **4·3CH_2Cl_2** (Figure 2b). The anionic chains of **5** are packed in a parallel disposition, with tetraphenylphosphonium cations between them, in an alternating fashion as shown in Figure 2c. This chain packing is comparable to that found in the silver derivative, $(PPh_4)_n[Rh_2(\mu\text{–}O_2CCH_2OEt)_4Ag(CN)_2]_n$ [60].

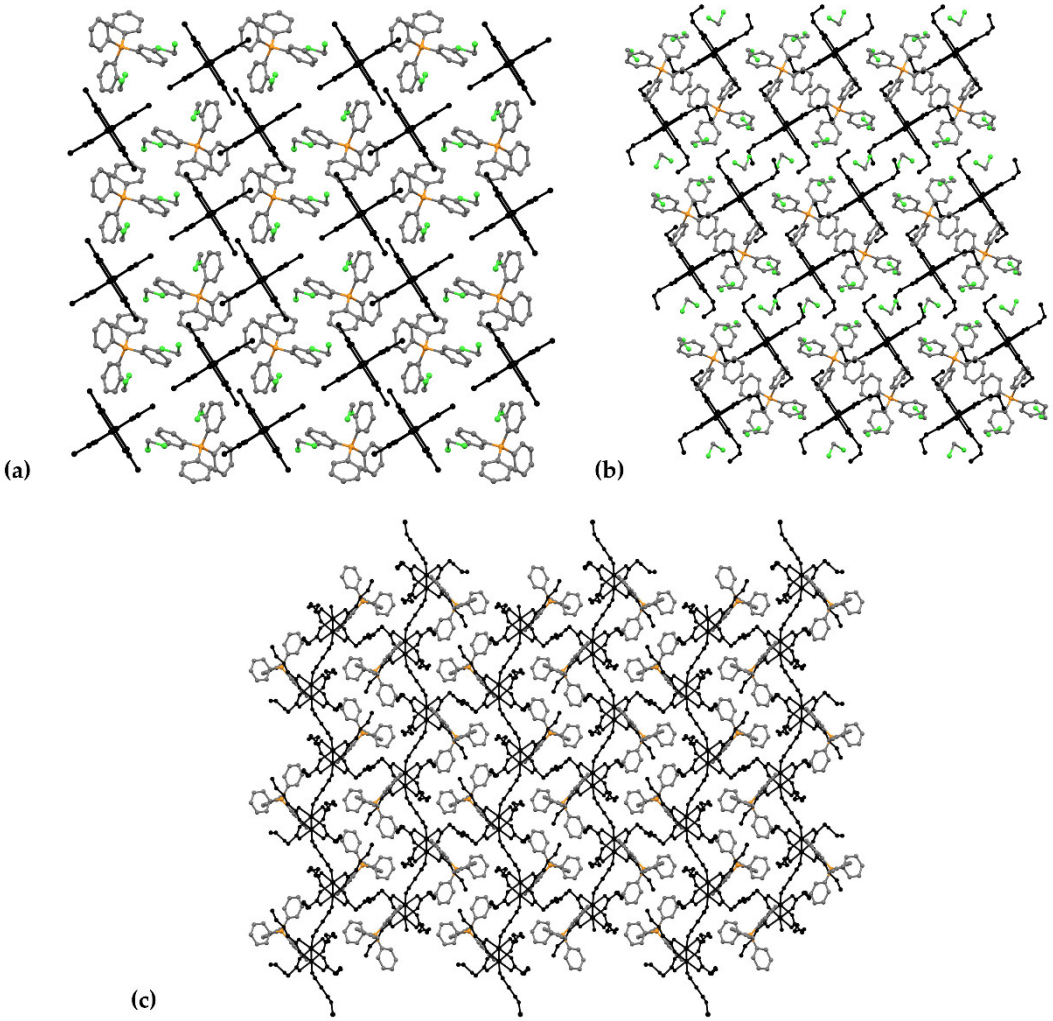

Figure 2. 3×3×3 packing along the *a* axis of the structures of **3·2CH_2Cl_2** (**a**), **4·3CH_2Cl_2** (**b**) and **5** (**c**) with the anionic chains of $[Rh_2(\mu\text{–}O_2CMe)_4Au(CN)_2]_n^{n-}$, $[Rh_2(\mu\text{–}O_2CCH_2OMe)_4Au(CN)_2]_n^{n-}$, and $[Rh_2(\mu\text{–}O_2CCH_2OEt)_4Au(CN)_2]_n^{n-}$, respectively, shown in black.

The supramolecular interactions between dirhodium units of the compounds are summarized in this paragraph. Several CH···O contacts between dirhodium molecules are observed in the structure of **1**. Each Rh1Rh1 unit is connected to four neighbor molecules and each Rh2Rh2 unit is connected to six neighbor molecules through this type of contacts (Figure S9). Two CH···O contacts

link couples of neighbor chains in the structure of **4·3CH$_2$Cl$_2$** (Figure S10), and two CH···N contacts connect the dirhodium discrete units in one direction in the structure of **7·2OCMe$_2$** (Figure S11). There is no significant interaction between dirhodium units in the structure of **3·2CH$_2$Cl$_2$**, **5**, and **6**. Moreover, the presence of tetraphenylphosphonium cations surrounding the dirhodium units does not allow the existence of Au–Au interactions in any structure. Thus, the shortest Au···Au distances are 8.7190(8), 9.747(2), 8.452(2), 7.8186(7), and 7.155(2) Å for **3·2CH$_2$Cl$_2$**, **4·3CH$_2$Cl$_2$**, **5**, **6**, and **7·2OCMe$_2$**, respectively.

There are also several weak interactions between dirhodium units and tetraphenylphosphonium cations and solvent molecules in the structures of **3·2CH$_2$Cl$_2$**, **4·3CH$_2$Cl$_2$**, **5**, **6**, and **7·2OCMe$_2$**. Each dirhodium unit of **3·2CH$_2$Cl$_2$** is connected to four tetraphenylphosphonium cations and two dichloromethane molecules through CH···O contacts. Moreover, an additional CH···N contact is established with another tetraphenylphosphonium cation (Figure S12). Similarly, each dirhodium unit of **4·3CH$_2$Cl$_2$** is connected to three tetraphenylphosphonium cations and three dichloromethane molecules through CH···O and CH···N contacts (Figure S13). Each dirhodium unit of **5** is connected to four tetraphenylphosphonium cations through CH···O contacts (Figure S14). Additionally, CH···π interactions are established with two neighboring tetraphenylphosphonium cations (Figure S15). The main cation-anion interactions in the molecular complex **6** are two CH···N contacts between the dicyanidoaurate(I) ligands in the axial positions of the paddlewheel units and two tetraphenylphosphonium cations (Figure S16). In the structure of **7·2OCMe$_2$** each dirhodium unit is connected to two acetone molecules through CH···O contacts and two tetraphenylphosphonium cations through CH···O and CH···N contacts (Figure S17).

The most remarkable interactions between tetraphenylphosphonium cations are pairs of weak CH···π interactions established between couples of cations in the structure of **3·2CH$_2$Cl$_2$** (3.127 Å) and **5** (3.146 Å) (Figures S18 and S19).

4. Conclusions

Complexes $(PPh_4)_n[Rh_2(\mu\text{–}O_2CR)_4Au(CN)_2]_n$ (R = Me (**3**), CH_2OMe (**4**), CH_2OEt (**5**)) show crystal structures formed by anionic wavy chains of $[Rh_2(\mu\text{–}O_2CR)_4Au(CN)_2]^-$ repetitive units in which the dicyanidoaurate(I) group acts as bridging ligand between the paddlewheel dirhodium(II) units. The formation of discrete anionic units, instead of anionic polymeric chains, in the complexes $(PPh_4)_2\{Rh_2(\mu\text{–}O_2CR)_4[Au(CN)_2]_2\}$ (R = CMe_3 (**6**), C_6H_4–*p*–CMe_3 (**7**)) has been attributed to the increase of the solubility in acetone due to the branched equatorial trimethylacetate and *tert*–butylbenzoate ligands. Significant intermolecular Au···Au interactions and, therefore, luminescent properties, are prevented due to the presence of the bulky tetraphenylphosphonium counterions, which are also involved in several CH···O and CH···N intermolecular contacts. The many similarities found in the crystal structures of **3·2CH$_2$Cl$_2$**, **5**, and **6** with their silver analogous indicate that silver and gold atoms do not play a substantial role in the crystal structures of this type of complexes when the same crystallization conditions are used. The structural description of these complexes contribute to increase the family of polymers of dirhodium carboxylates with $[Au(CN)_2]^-$. This knowledge could be useful for the design of future polymers with potential applications in several areas as catalysis or bioinorganic chemistry.

Supplementary Materials: The following are available online at www.mdpi.com/2073-4360/12/9/1868/s1, Figure S1: Representation of the asymmetric unit of $[Rh_2(\mu\text{–}O_2CCH_2OMe)_4(THF)_2]$ (**1**). Table S1: Selected bond lengths and angles for $[Rh_2(\mu\text{–}O_2CCH_2OMe)_4(THF)_2]$ (**1**). Figure S2: Representation of the asymmetric unit of $\{(PPh_4)[Rh_2(\mu\text{–}O_2CMe)_4Au(CN)_2]\cdot 2CH_2Cl_2\}_n$ (**3·2CH$_2$Cl$_2$**). Table S2: Selected bond lengths and angles for $\{(PPh_4)[Rh_2(\mu\text{–}O_2CMe)_4Au(CN)_2]\cdot 2CH_2Cl_2\}_n$ (**3·2CH$_2$Cl$_2$**). Figure S3: Representation of the asymmetric unit of $\{(PPh_4)[Rh_2(\mu\text{–}O_2CCH_2OMe)_4Au(CN)_2]\cdot 3CH_2Cl_2\}_n$ (**4·3CH$_2$Cl$_2$**). Table S3: Selected bond lengths and angles for $\{(PPh_4)[Rh_2(\mu\text{–}O_2CCH_2OMe)_4Au(CN)_2]\cdot 3CH_2Cl_2\}_n$ (**4·3CH$_2$Cl$_2$**). Figure S4: Representation of the asymmetric unit of $(PPh_4)_n[Rh_2(\mu\text{–}O_2CCH_2OEt)_4Au(CN)_2]_n$ (**5**). Table S4: Selected bond lengths and angles for $(PPh_4)_n[Rh_2(\mu\text{–}O_2CCH_2OEt)_4Au(CN)_2]_n$ (**5**). Figure S5: Representation of the asymmetric unit of $(PPh_4)_2\{Rh_2(\mu\text{–}O_2CCMe_3)_4[Au(CN)_2]_2\}$ (**6**). Table S5: Selected bond lengths and angles for $(PPh_4)_2\{Rh_2(\mu\text{-}O_2CCMe_3)_4[Au(CN)_2]_2\}$ (**6**). Figure S6: Representation of the asymmetric unit of $(PPh_4)_2\{Rh_2(\mu\text{–}O_2CC_6H_4\text{–}p\text{–}CMe_3)_4[Au(CN)_2]_2\}\cdot 2OCMe_2$ (**7·2OCMe$_2$**). Table S6: Selected bond lengths and angles for $(PPh_4)_2\{Rh_2(\mu\text{–}O_2CC_6H_4\text{–}p\text{–}$

$CMe_3)_4[Au(CN)_2]_2\}\cdot 2OCMe_2$ (**7·2OCMe$_2$**). Figure S7: 3×3×3 packing along the *c* axis of the structure of **6**. Figure S8: 3×3×3 packing along the *b* axis of the structure of **7·2OCMe$_2$**. Figure S9: View of the CH···O contacts between Rh1-Rh1 (top) and Rh2-Rh2 (bottom) dirhodium units and neighboring units in the structure of **1**. Figure S10: View of the CH···O contacts between neighbor chains in the structure of **4·3CH$_2$Cl$_2$**. Figure S11: View of the CH···N contacts between neighbor dirhodium units in the structure of **7·2OCMe$_2$**. Figure S12: View of the CH···O and CH···N contacts between dirhodium units and tetraphenylphosphonium cations and dichloromethane molecules in the structure of **3·2CH$_2$Cl$_2$**. Figure S13: View of the CH···O and CH···N contacts between dirhodium units and tetraphenylphosphonium cations and dichloromethane molecules in the structure of **4·3CH$_2$Cl$_2$**. Figure S14: View of the CH···O contacts between dirhodium units and tetraphenylphosphonium cations in the structure of **5**. Figure S15: View of the CH···π interactions between dirhodium units and tetraphenylphosphonium cations in the structure of **5**. Figure S16: View of the CH···N contacts between dirhodium units and tetraphenylphosphonium cations in the structure of **6**. Figure S17: View of the CH···O and CH···N contacts between dirhodium units and tetraphenylphosphonium cations and acetone molecules in the structure of **7·2OCMe$_2$**. Figure S18: View along the *a* axis of the closest tetraphenylphosphonium cations and the CH···π interactions between them in the structure of of **3·2CH$_2$Cl$_2$**. Figure S19: View along the *a* axis of the closest tetraphenylphosphonium cations and the CH···π interactions between them in the structure of **5**.

Author Contributions: J.L.P. and R.J.-A designed the study, E.F.-B., P.C., and L.A.G. performed the synthesis and general characterization of the compounds, R.G.-P assisted in the experiments, P.D.-M and M.C. were responsible for the crystal structure characterization, all authors contributed to the analysis and interpretation of data, and M.C., R.G.-P., and R.J.-A. All authors have read and agreed to the published version of the manuscript.

Funding This research was funded by the Spanish Ministerio de Economía y Competitividad (project CTQ2015-63858-P, MINECO/FEDER) and Comunidad de Madrid (project B2017/BMD-3770-CM).

Conflicts of Interest: The authors declare no conflicts of interest. The funders had no role in the design of the study; in the collection, analyses, or interpretation of data; in the writing of the manuscript; or in the decision to publish the results.

References

1. Cotton, F.A.; Walton, R.A. *Multiple Bonds between Metal Atoms*, 2nd ed.; Wiley: New York, NY, USA, 1982.
2. Cotton, F.A.; Murillo, C.; Walton, R.A. *Multiple Bonds between Metal Atoms*, 3rd ed.; Springer: New York, NY, USA, 2005.
3. Liddle, S.T.; *Molecular Metal-Metal Bonds: Compounds, Synthesis, Properties*; Wiley: Weinheim, Germany, 2015.
4. Hayashi, H.; Uchida, T. Nitrene Transfer Reactions for Asymmetric C-H Amination: Recent Development. *Eur. J. Org. Chem.* **2020**, *2020*, 909–916, doi:10.1002/ejoc.201901562.
5. Li, S.-J.; Li, X.; Mo, H.; Qu, L.-B.; Wei, D.; Lan, Y. With metal or not? a computationally predicted rule for a dirhodium catalyst in [3+3] cycloadditions of triazole with thiirane. *Chem. Commun.* **2020**, *56*, 4732–4735, doi:10.1039/d0cc01293a.
6. Davies, H.M.L.; Liao, K. Dirhodium tetracarboxylates as catalysts for selective intermolecular C–H functionalization. *Nat. Rev. Chem.* **2019**, *3*, 347–360, doi:10.1038/s41570-019-0099-x.
7. Kataoka, Y.; Yano, N.; Kohara, Y.; Tsuji, T.; Inoue, S.; Kawamoto, T. Experimental and Theoretical Study of Photochemical Hydrogen Evolution Catalyzed by Paddlewheel-Type Dirhodium Complexes with Electron Withdrawing Carboxylate Ligands. *ChemCatChem* **2019**, *11*, 6218–6226, doi:10.1002/cctc.201901534.
8. Levchenko, V.; Sundsli, B.; Øien-Ødegaard, S.; Tilset, M.; Hansen, F.K.; Bonge-Hansen, T. Bottom-Up Synthesis of Acrylic and Styrylic RhII Carboxylate Polymer Beads: Solid-Supported Analogs of $Rh_2(OAc)_4$. *Eur. J. Org. Chem.* **2018**, *2018*, 6150–6157, doi:10.1002/ejoc.201800953.
9. Kornecki, K.P.; Briones, J.F.; Boyarskikh, V.; Fullilove, F.; Autschbach, J.; Schrote, K.E.; Lancaster, K.M.; Davies, H.M.L.; Berry, J.F. Direct Spectroscopic Characterization of a Transitory Dirhodium Donor-Acceptor Carbene Complex. *Sci.* **2013**, *342*, 351–354, doi:10.1126/science.1243200.
10. Hansen, J.; Davies, H.M.L. High symmetry dirhodium(II) paddlewheel complexes as chiral catalysts. *Coord. Chem. Rev.* **2008**, *252*, 545–555, doi:10.1016/j.ccr.2007.08.019.
11. Sokolov, M.N.; Adonin, S.A.; Peresypkina, E.V.; Abramov, P.A.; Smolentsev, A.I.; Potemkin, D.; Snytnikov, P.; Fedin, V.P. Reactions of rhodium (II) acetate with non-lacunary Keggin and Dawson polyoxoanions and related catalytic studies. *Inorganica Chim. Acta* **2013**, *394*, 656–662, doi:10.1016/j.ica.2012.07.028.

12. Berndt, J.P.; Radchenko, Y.; Becker, J.; Logemann, C.; Bhandari, D.R.; Hrdina, R.; Schreiner, P.R. Site-selective nitrenoid insertions utilizing postfunctionalized bifunctional rhodium(II) catalysts. *Chem. Sci.* **2019**, *10*, 3324–3329, doi:10.1039/c8sc05733h.
13. Ferraro, G.; Pratesi, A.; Messori, L.; Merlino, A. Protein interactions of dirhodium tetraacetate: a structural study. *Dalton Trans.* **2020**, *49*, 2412–2416, doi:10.1039/c9dt04819g.
14. Brunskill, V.; Garcia, A.E.; Jalilehvand, F.; Gelfand, B.S.; Wu, M. Reaction of dirhodium(II) tetraacetate with *S*-methyl-*L*-cysteine. *J. Coord. Chem.* **2019**, *72*, 2177–2188, doi:10.1080/00958972.2019.1651845.
15. Lewis, J.C. Beyond the Second Coordination Sphere: Engineering Dirhodium Artificial Metalloenzymes To Enable Protein Control of Transition Metal Catalysis. *Accounts Chem. Res.* **2019**, *52*, 576–584, doi:10.1021/acs.accounts.8b00625.
16. Knoll, J.D.; Turro, C. Control and utilization of ruthenium and rhodium metal complex excited states for photoactivated cancer therapy. *Coord. Chem. Rev.* **2015**, 110–126, doi:10.1016/j.ccr.2014.05.018.
17. Leung, C.-H.; Zhong, H.-J.; Chan, D.S.-H.; Ma, D.-L. Bioactive iridium and rhodium complexes as therapeutic agents. *Coord. Chem. Rev.* **2013**, *257*, 1764–1776, doi:10.1016/j.ccr.2013.01.034.
18. Furukawa, S.; Horike, N.; Kondo, M.; Hijikata, Y.; Carné-Sánchez, A.; Larpent, P.; Louvain, N.; Diring, S.; Sato, H.; Matsuda, R.; et al. Rhodium–Organic Cuboctahedra as Porous Solids with Strong Binding Sites. *Inorg. Chem.* **2016**, *55*, 10843–10846, doi:10.1021/acs.inorgchem.6b02091.
19. Kataoka, Y.; Kataoka, K.S.; Murata, H.; Handa, M.; Mori, W.; Kawamoto, T. Synthesis and characterizations of a paddlewheel-type dirhodium-based photoactive porous metal-organic framework. *Inorg. Chem. Commun.* **2016**, *68*, 37–41, doi:10.1016/j.inoche.2016.04.009.
20. Zhang, J.; Kosaka, W.; Kitagawa, S.; Takata, M.; Miyasaka, H. In Situ Tracking of Dynamic NO Capture through a Crystal-to-Crystal Transformation from a Gate-Open-Type Chain Porous Coordination Polymer to a NO-Adducted Discrete Isomer. *Chem. Eur. J.* **2019**, *25*, 3020–3031, doi:10.1002/chem.201805833.
21. Tsuchiya, T.; Umemura, R.; Kaminaga, M.; Kushida, S.; Ohkubo, K.; Noro, S.-I.; Mazaki, Y. Paddlewheel Complexes with Azulenes: Electronic Interaction between Metal Centers and Equatorial Ligands. *ChemPlusChem* **2019**, *84*, 655–664, doi:10.1002/cplu.201800513.
22. Liu, G.; Wang, Y.; Zhu, B.; Zhang, L.; Su, C.-Y. A porous metal–organic aerogel based on dirhodium paddle-wheels as an efficient and stable heterogeneous catalyst towards the reduction reaction of aldehydes and ketones. *New J. Chem.* **2018**, *42*, 11358–11363, doi:10.1039/c8nj01784k.
23. Zhu, B.; Liu, G.; Chen, L.; Qiu, L.; Chen, L.; Zhang, J.; Zhang, L.; Barboiu, M.; Si, R.; Su, C.-Y. Metal–organic aerogels based on dinuclear rhodium paddle-wheel units: design, synthesis and catalysis. *Inorg. Chem. Front.* **2016**, *3*, 702–710, doi:10.1039/C5QI00272A.
24. Rossi, L.; Huck-Iriart, C.; Castro, M.A.; Cukiernik, F.D. Liquid-crystalline coordination polymers based on tetra(alkoxybenzoato)dirhodium(II) complexes axially linked by tetrazine, phenazine and 4,4′-bipyridine. *J. Coord. Chem.* **2017**, *70*, 3633–3649, doi:10.1080/00958972.2017.1403594.
25. Rusjan, M.; Donnio, B.; Guillon, D.; Cukiernik, F.D. Liquid-Crystalline Materials Based on Rhodium Carboxylate Coordination Polymers: Synthesis, Characterization and Mesomorphic Properties of Tetra(alkoxybenzoato)dirhodium(II) Complexes and Their Pyrazine Adducts. *Chem. Mater.* **2002**, *14*, 1564–1575, doi:10.1021/cm0109995.
26. Sarkar, M.; Daw, P.; Ghatak, T.; Bera, J.K. Amide-Functionalized Naphthyridines on a Rh^{II}-Rh^{II} Platform: Effect of Steric Crowding, Hemilability, and Hydrogen-Bonding Interactions on the Structural Diversity and Catalytic Activity of Dirhodium(II) Complexes. *Chem. Eur. J.* **2014**, *20*, 16537–16549, doi:10.1002/chem.201402936.
27. Amo-Ochoa, P.; Jimenez, R.; Perles, J.; Torres, M.R.; Gennari, M.; Zamora, F. Structural Diversity in Paddlewheel Dirhodium(II) Compounds through Ionic Interactions: Electronic and Redox Properties. *Cryst. Growth Des.* **2013**, *13*, 4977–4985, doi:10.1021/cg4011532.
28. Filatov, A.S.; Rogachev, A.Y.; Petrukhina, M.A. Gas-Phase Assembling of Dirhodium Units into a Novel Organometallic Ladder: Structural and DFT Study. *Cryst. Growth Des.* **2006**, *6*, 1479–1484, doi:10.1021/cg060118c.
29. Cooke, M.W.; Hanan, G.S.; Loiseau, F.; Campagna, S.; Watanabe, M.; Tanaka, Y. The Structural and Functional Roles of Rhodium(II)-Rhodium(II) Dimers in Multinuclear Ruthenium(II) Complexes. *Angew. Chem. Int. Ed.* **2005**, *44*, 4881–4884, doi:10.1002/anie.200500392.

30. Takamizawa, S.; Nakata, E.-I.; Yokoyama, H.; Mochizuki, K.; Mori, W. Carbon Dioxide Inclusion Phases of a Transformable 1D Coordination Polymer Host $[Rh_2(O_2CPh)_4(pyz)]_n$. *Angew. Chem. Int. Ed.* **2003**, *42*, 4331–4334, doi:10.1002/anie.200351368.
31. Cotton, F.A.; Dikarev, E.V.; Petrukhina, M.A.; Schmitz, M.; Stang, P.J. Supramolecular Assemblies of Dimetal Complexes with Polydentate N-Donor Ligands: From a Discrete Pyramid to a 3D Channel Network. *Inorg. Chem.* **2002**, *41*, 2903–2908, doi:10.1021/ic020051s.
32. Cotton, F.A.; Dikarev, E.V.; Petrukhina, M.A. Using Structures Formed by Dirhodium Tetra(trifluoroacetate) with Polycyclic Aromatic Hydrocarbons to Prospect for Maximum π-Electron Density: Hückel Calculations Get It Right. *J. Am. Chem. Soc.* **2001**, *123*, 11655–11663, doi:10.1021/ja016801z.
33. Kataoka, Y.; Fukumoto, R.; Yano, N.; Atarashi, D.; Tanaka, H.; Kawamoto, T.; Handa, M. Synthesis, Characterization, Absorption Properties, and Electronic Structures of Paddlewheel-Type Dirhodium(II) Tetra–μ–(n–naphthoate) Complexes: An Experimental and Theoretical Study. *Mol.* **2019**, *24*, 447, doi:10.3390/molecules24030447.
34. Anderson, B.G.; Cressy, D.; Patel, J.J.; Harris, C.F.; Yap, G.P.A.; Berry, J.F.; Darko, A. Synthesis and Catalytic Properties of Dirhodium Paddlewheel Complexes with Tethered, Axially Coordinating Thioether Ligands. *Inorg. Chem.* **2019**, *58*, 1728–1732, doi:10.1021/acs.inorgchem.8b02627.
35. Belman, O.F.G.; Varela, Y.; Flores-Alamo, M.; Wróbel, K.; Gutiérrez-Granados, S.; Peralta-Hernández, J.M.; Jimenez-Halla, J.O.C.; Serrano, O. Microwave-Assisted Synthesis and Characterization of $[Rh_2(OAc)_4(L)_2]$ Paddlewheel Complexes: A Joint Experimental and Computational Study. *Int. J. Inorg. Chem.* **2017**, *2017*, 1–12, doi:10.1155/2017/5435436.
36. Ye, Q.-S.; Li, X.-N.; Jin, Y.; Yu, J.; Chang, Q.-W.; Jiang, J.; Yan, C.-X.; Li, J.; Liu, W. Synthesis, crystal structures and catalytic activity of tetrakis(acetato)dirhodium(II) complexes with axial picoline ligands. *Inorganica Chim. Acta* **2015**, *434*, 113–120, doi:10.1016/j.ica.2015.05.017.
37. Cmoch, P.; Głaszczka, R.; Jazwinski, J.; Kamieński, B.; Senkara, E. Adducts of nitrogenous ligands with rhodium(II) tetracarboxylates and tetraformamidinate: NMR spectroscopy and density functional theory calculations. *Magn. Reson. Chem.* **2013**, *52*, 61–68, doi:10.1002/mrc.4035.
38. Kataoka, Y.; Yano, N.; Shimodaira, T.; Yan, Y.; Yamasaki, M.; Tanaka, H.; Omata, K.; Kawamoto, T.; Handa, M. Paddlewheel-Type Dirhodium Tetrapivalate Based Coordination Polymer: Synthesis, Characterization, and Self-Assembly and Disassembly Transformation Properties. *Eur. J. Inorg. Chem.* **2016**, *2016*, 2810–2815, doi:10.1002/ejic.201600197.
39. Fritsch, N.; Wick, C.R.; Waidmann, T.; Dral, P.O.; Tucher, J.; Heinemann, F.W.; Shubina, T.; Clark, T.; Burzlaff, N. Multiply Bonded Metal(II) Acetate (Rhodium, Ruthenium, and Molybdenum) Complexes with the trans-1,2-Bis(*N*-methylimidazol-2-yl)ethylene Ligand. *Inorg. Chem.* **2014**, *53*, 12305–12314, doi:10.1021/ic501435a.
40. Dikarev, E.V.; Filatov, A.S.; Clerac, R.; Petrukhina, M.A. Unligated Diruthenium(II,II) Tetra(trifluoroacetate): The First X-ray Structural Study, Thermal Compressibility, Lewis Acidity, and Magnetism. *Inorg. Chem.* **2006**, *45*, 744–751, doi:10.1021/ic051537m.
41. Dikarev, E.V.; Shpanchenko, R.V.; Andreini, K.W.; Block, S.; Jin; Petrukhina, M.A. Powder Diffraction Study of a Coordination Polymer Comprised of Rigid Building Blocks: $[Rh_2(O_2CCH_3)_4{\cdot}\mu^2{-}Se_2C_5H_8{-}Se,Se']_\infty$. *Inorg. Chem.* **2004**, *43*, 5558–5563, doi:10.1021/ic049497u.
42. Uemura, K. Magnetic behavior in heterometallic one-dimensional chains or octanuclear complex regularly aligned with metal–metal bonds as –Rh–Rh–Pt–Cu–Pt. *J. Mol. Struct.* **2018**, *1162*, 31–36, doi:10.1016/j.molstruc.2018.02.078.
43. Uemura, K. One-dimensional complexes extended by unbridged metal–metal bonds based on a HOMO–LUMO interaction at the d_{z^2} orbital between platinum and heterometal atoms. *Dalton Trans.* **2017**, *46*, 5474–5492, doi:10.1039/C6DT04515D.
44. Yamada, T.; Uemura, K.; Ebihara, M. Heterometallic one-dimensional chain with tetradeca metal repetition constructed by amidate bridged dirhodium and pivalate bridged diplatinum complexes influenced by hydrogen bonding. *Dalton Trans.* **2016**, *45*, 12322–12328, doi:10.1039/C6DT01601D.
45. Uemura, K.; Yamada, T.; Kanbara, T.; Ebihara, M. Acetamidate-bridged paddlewheel dirhodium complex sandwiched by mononuclear platinum complexes with axial metal–metal bonds affording neutral heterometallic one-dimensional alignments. *Inorganica Chim. Acta* **2015**, *424*, 194–201, doi:10.1016/j.ica.2014.08.041.

46. Uemura, K.; Kanbara, T.; Ebihara, M. Two Types of Heterometallic One-Dimensional Alignment Composed of Acetamidate-Bridged Dirhodium and Pivalamidate-Bridged Diplatinum Complexes. *Inorg. Chem.* **2014**, *53*, 4621–4628, doi:10.1021/ic500305n.
47. Uemura, K.; Ebihara, M. Paramagnetic One-Dimensional Chains Comprised of Trinuclear Pt–Cu–Pt and Paddlewheel Dirhodium Complexes with Metal–Metal Bonds. *Inorg. Chem.* **2013**, *52*, 5535–5550, doi:10.1021/ic400470g.
48. Yang, Z.; Ebihara, M.; Kawamura, T. One-dimensional chain structures constructed from tetra(acetamidato)dirhodium(II,III) complexes and square planar platinum and palladium complexes. *Inorganica Chim. Acta* **2006**, *359*, 2465–2471, doi:10.1016/j.ica.2006.02.034.
49. Heyduk, A.F.; Krodel, D.J.; Meyer, E.E.; Nocera, D.G. A Luminescent Heterometallic Dirhodium−Silver Chain. *Inorg. Chem.* **2002**, *41*, 634–636, doi:10.1021/ic015562d.
50. Uemura, K.; Ebihara, M. One-Dimensionally Extended Paddlewheel Dirhodium Complexes from Metal–Metal Bonds with Diplatinum Complexes. *Inorg. Chem.* **2011**, *50*, 7919–7921, doi:10.1021/ic200786k.
51. Qin, Y.-L.; Yang, B.-W.; Wang, G.-F.; Sun, H. A cyanide-bridged heterometallic coordination polymer constructed from square-planar $[Ni(CN)_4]^{2-}$: synthesis, crystal structure, thermal decomposition, electron paramagnetic resonance (EPR) spectrum and magnetic properties. *Acta Crystallogr. Sect. C Struct. Chem.* **2016**, *72*, 555–560, doi:10.1107/s2053229616009372.
52. Alexandrov, E.V.; Virovets, A.V.; Blatov, V.A.; Peresypkina, E.V.; Alexrov, E.V. Topological Motifs in Cyanometallates: From Building Units to Three-Periodic Frameworks. *Chem. Rev.* **2015**, *115*, 12286–12319, doi:10.1021/acs.chemrev.5b00320.
53. Marinescu, G.; Madalan, A.M.; Andruh, M. New heterometallic coordination polymers based on zinc(II) complexes with Schiff-base ligands and dicyanometallates: synthesis, crystal structures, and luminescent properties. *J. Coord. Chem.* **2015**, *68*, 479–490, doi:10.1080/00958972.2014.997721.
54. Gör, K.; Tursun, M.; Keşan, G.; Kürkçüoğlu, G.S.; Rhyman, L.; Parlak, C.; Ramasami, P.; Yeşilel, O.Z.; Büyükgüngör, O. Novel Cyanide-Bridged Heterometallic Two-Dimensional Complex of 3-Methylpyridazine: Synthesis, Crystallographical, Vibrational, Thermal and DFT Studies. *J. Inorg. Organomet. Polym. Mater.* **2015**, *25*, 1205–1217, doi:10.1007/s10904-015-0229-y.
55. Wang, S.; Ding, X.-H.; Zuo, J.-L.; You, X.-Z.; Huang, W. Tricyanometalate molecular chemistry: A type of versatile building blocks for the construction of cyano-bridged molecular architectures. *Coord. Chem. Rev.* **2011**, *255*, 1713–1732, doi:10.1016/j.ccr.2011.01.057.
56. Baril-Robert, F.; Li, X.; Katz, M.J.; Geisheimer, A.R.; Leznoff, D.B.; Patterson, H.H. Changes in Electronic Properties of Polymeric One-Dimensional $\{[M(CN)_2]^-\}_n$ (M = Au, Ag) Chains Due to Neighboring Closed-Shell Zn(II) or Open-Shell Cu(II) Ions. *Inorg. Chem.* **2011**, *50*, 231–237, doi:10.1021/ic101841a.
57. Kennon, B.S.; Stone, K.H.; Stephens, P.W.; Miller, J.S. Interpenetrating diruthenium tetraformate monocation, $[Ru^{II/III}_2(O_2CH)_4]^+$, based 3-D molecule-based magnets. *CrystEngComm* **2009**, *11*, 2185–2191, doi:10.1039/b906437k.
58. Contakes, S.M.; Klausmeyer, K.K.; Rauchfuss, T.B. Coordination Solids Derived from $Cp^*M(CN)_3^-$ (M = Rh, Ir). *Inorg. Chem.* **2000**, *39*, 2069–2075, doi:10.1021/ic991037r.
59. Amo-Ochoa, P.; Delgado, S.; Gallego, A.; Gómez-García, C.J.; Jimenez, R.; Martínez, G.; Perles, J.; Torres, M.R.; Martínez-García, G. Structure and Properties of One-Dimensional Heterobimetallic Polymers Containing Dicyanoaurate and Dirhodium(II) Fragments. *Inorg. Chem.* **2012**, *51*, 5844–5849, doi:10.1021/ic3004307.
60. Cruz, P.; Fernandez-Bartolome, E.; Cortijo, M.; Delgado-Martínez, P.; González-Prieto, R.; Priego, J.L.; Torres, M.R.; Jimenez, R. Synthesis and Structural Characterization of a Series of One-Dimensional Heteronuclear Dirhodium-Silver Coordination Polymers. *Polym.* **2019**, *11*, 111, doi:10.3390/polym11010111.
61. Prior, D.; Cortijo, M.; González-Prieto, R.; Herrero, S.; Jiménez-Aparicio, R.; Perles, J.; Priego, J.L. Linear One-Dimensional Coordination Polymers Constructed by Dirhodium Paddlewheel and Tetracyanido-Metallate Building Blocks. *Cryst.* **2019**, *9*, 614, doi:10.3390/cryst9120614.
62. Katz, M.J.; Sakai, K.; Leznoff, D.B. The use of aurophilic and other metal–metal interactions as crystal engineering design elements to increase structural dimensionality. *Chem. Soc. Rev.* **2008**, *37*, 1884, doi:10.1039/b709061g.
63. Zaręba, J.K.; Białek, M.J.; Janczak, J.; Zoń, J.; Dobosz, A. Extending the Family of Tetrahedral Tectons: Phenyl Embraces in Supramolecular Polymers of Tetraphenylmethane-based Tetraphosphonic Acid Templated by Organic Bases. *Cryst. Growth Des.* **2014**, *14*, 6143–6153, doi:10.1021/cg501348g.

64. Ali, B.F.; Dance, I.G.; Scudder, M.; Craig, D. Dimorphs of $(Ph_4P)_2[Cd_2(SPh)_6]$: Crystal Packing Analyses and the Interplay of Intermolecular and Intramolecular Energies. *Cryst. Growth Des.* **2002**, *2*, 601–607, doi:10.1021/cg0255422.
65. Cotton, F.A.; Felthouse, T.R. Structural studies of three tetrakis(carboxylato)dirhodium(II) adducts in which carboxylate groups and axial ligands are varied. *Inorg. Chem.* **1980**, *19*, 323–328, doi:10.1021/ic50204a010.
66. Mikuriya, M.; Yamamoto, J.; Ishida, H.; Yoshioka, D.; Handa, M. Preparation and Crystal Structure of Tetrakis(μ-pivalato-O,O′)bis[(pivalic acid-O)rhodium(II)]. *X-ray Struct. Anal. Online* **2011**, *27*, 7–8, doi:10.2116/xraystruct.27.7.
67. Aquino, M.A. Diruthenium and diosmium tetracarboxylates: synthesis, physical properties and applications. *Coord. Chem. Rev.* **1998**, *170*, 141–202, doi:10.1016/s0010-8545(97)00079-9.
68. Spek, A.L. PLATONSQUEEZE: a tool for the calculation of the disordered solvent contribution to the calculated structure factors. *Acta Crystallogr. Sect. C Struct. Chem.* **2015**, *71*, 9–18, doi:10.1107/s2053229614024929.
69. Kim, Y.; Kim, S.-J.; Nam, W. A ferric-cyanide-bridged one-dimensional dirhodium complex with (18-crown-6)potassium cations. *Acta Crystallogr. Sect. C Cryst. Struct. Commun.* **2001**, *57*, 266–268, doi:10.1107/s0108270100019776.
70. Lu, J.; Harrison, W.T.A.; Jacobson, A.J. Synthesis and crystal structure of the two-dimensional polymer $K_3Co(CN)_6{\cdot}2Rh_2(O_2CMe)_4$. *Chem. Commun.* **1996**, 399–400, doi:10.1039/cc9960000399.